

IN-34
140763
P.18

Physical Vapor Transport of Mercurous Chloride Under a Nonlinear Thermal Profile

Christophe Mennetrier, Walter M.B. Duval
Lewis Research Center
Cleveland, Ohio

and

Narsingh B. Singh
Westinghouse Science and Technology Center
Pittsburgh, Pennsylvania

November 1992

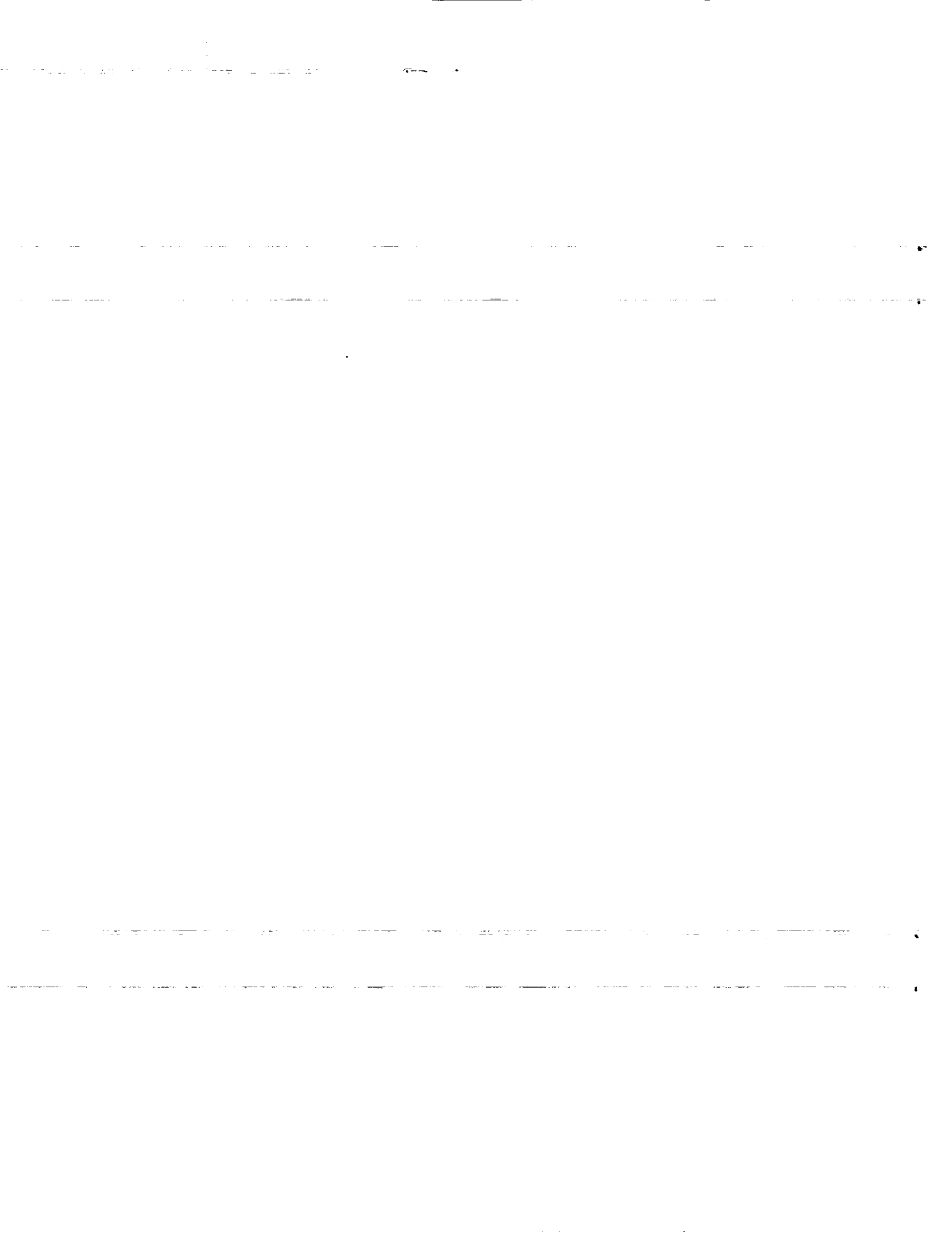
(NASA-TM-105920) PHYSICAL VAPOR
TRANSPORT OF MERCUROUS CHLORIDE
UNDER A NONLINEAR THERMAL PROFILE
(NASA) 18 p

N93-16612

Unclas

NASA

G3/34 0140763



PHYSICAL VAPOR TRANSPORT OF MERCUROUS CHLORIDE UNDER A NONLINEAR THERMAL PROFILE

Christophe Mennetrier *, *Walter M.B. Duval*

NASA Lewis Research Center
Cleveland, Ohio 44135

Narsingh B. Singh

Westinghouse Science and Technology Center
Pittsburgh, Pennsylvania 15235

I INTRODUCTION

Physical Vapor Transport (PVT) has been examined numerically for conditions where the boundary of the enclosure is subjected to a nonlinear thermal profile. Prior numerical studies have ^(3-9,11-13,17,20) considered the effects of thermal and solutal convection, under various thermal boundary conditions, and for conducting (linear temperature profile) and adiabatic walls. These studies showed that convection is responsible for the non-uniformity of the transport flux at the interface. It was also shown that for conducting walls, when thermal convection is dominant, the maximum flux occurs between 120 ° and 130 ° (depending on the aspect ratio) from the bottom-heated configuration. Extremet et al. ⁽²³⁾ used a similar set of governing equations to investigate multizone PVT. They emphasized the importance of solutal convection and showed that it can compete with thermal convection to produce multiple cell patterns. Zappoli ⁽¹⁹⁾ demonstrated that the release of latent heat associated with the evaporation and the condensation of the gas at both interfaces can affect the concentration field near the interface. However, the actual thermodynamical dependency of the vapor pressure of nutrient with temperature of the interface is often discarded. The case for mercurous chloride (Hg_2Cl_2) in which the thermodynamical dependency of the vapor pressure law is taken into account has been studied ⁽²⁶⁾. It was shown that solutal convection is the dominant mode of transport. These studies included heat conduction in the crystal, with conducting walls. It was also shown that the interface temperature deviates from a constant value when a thermal gradient is present in the crystal. Kassemi and Duval ^(24,25) have shown that when internal and surface radiation become important in the process, non-uniformities of interfacial mass flux can occur. These past numerical studies indicate that under earth gravity, it is difficult to obtain a diffusive flow for the horizontal configuration.

Experimental works in PVT have focused on determining transport rates. Conder et al. ⁽¹⁸⁾ have determined experimentally that the transport rate of mercurous iodide is controlled by mass transfer in the vapor phase. They also showed that the transport rate decreases with the pressure of carrier gas such as argon, and increases with the

* Visiting Research Associate, Ecole Nationale Supérieure des Mines, France

temperature difference between source and sink. In an early work on chemical vapor transport (CVT), Chandra and Weidemeier ⁽¹⁰⁾ observed the shift of the maximum transport rate away from the horizontal configuration, and also showed the transport rate increased with the pressure of nutrient (i.e. temperature difference). Related to natural convection in PVT, Schiroky and Rosenberger ⁽¹²⁾ experimentally studied free convection of gases in a horizontal cylinder with differentially heated end walls and obtained velocity measurements with Laser Doppler Velocimetry. At high Rayleigh numbers, pronounced 3-D flow behavior was observed. These measurements were later confirmed numerically by Smutek et al. ⁽¹⁷⁾ with a 3-D model.

The goal of this work is to numerically study more extensively solutal convection in PVT of mercurous chloride subjected to a nonlinear temperature profile. The effect of thermal radiation is neglected. We include the effect of the angle of tilt, and in contrast to the results obtained by Markham and Rosenberger ⁽¹³⁾ for the case of thermal convection, we consider the case when solutal convection is dominant. For practical crystal growth applications, it is sometimes necessary to grow the crystal with a nonlinear thermal profile. We will therefore input a measured thermal profile ⁽²⁷⁾, with an overheat to avoid heterogeneous condensation of the vapor on the walls (as we explain in paragraph II). Our studies indicate that this profile destabilizes the flow field when thermal convection is dominant for the vertical configuration. However, when solutal convection dominates, density gradients associated with solute gradients stabilize the flow field for the bottom-heated configuration. Finally, we investigate various cases applicable to the microgravity environment, and we deduce the gravity levels required to restore a diffusive mode of mass transfer and avoid non-uniformity of the interfacial mass flux distribution for the horizontal configuration.

II APPLICATIONS AND CRYSTAL GROWTH TECHNIQUE

The mercurous halides have recently become important because of their application in acousto-optic and opto-electronic devices. The properties that make this class of materials important are:

- a) the large spectral transmission range,
- b) the large photo-elastic coefficient,
- c) the very high acousto-optic figure of merit,
- d) the extremely low acoustic velocity, and
- e) the reasonably low acoustic attenuation.

These halides belong to the tetragonal (D4h) crystal class and are positively uniaxial with large birefringence. The refractive indices for Hg_2Cl_2 are 2.621 and 1.962 (birefringent material), the transmission range is $0.36 \mu m$ to $20 \mu m$. This wide optical transmission range is very unusual and potentially very useful for wideband spectroscopic devices.

The need for high optical quality crystals comes from communication applications of the device for which mercurous chloride appears to have great potential. Of the metal halides, mercurous chloride has the slowest shear acoustic velocity in the [110] direction ($347 ms^{-1}$). Also, the acoustic attenuation for high quality crystals appears to be reasonably low: $376 dBcm^{-1}GHz^{-2}$. These properties are well suited for fabrication of Bragg cells which can offer high resolution, high diffraction efficiency, and high

dynamic range.

Mercurous halides decompose to mercury and mercuric halide at the melting point ($Hg_2X_2 \rightarrow Hg + HgX_2$). The existence of the two liquid fields and compositional stratification largely preclude the solidification of large Hg_2X_2 crystals by conventional melt growth techniques. However, mercurous halides exhibit reasonably high vapor pressure at low temperature, and crystal growth by vapor transport can be accomplished at rates well within practical range.

Because of heterogeneous condensation on the walls, a linear thermal gradient is sometimes inadequate to grow mercurous chloride crystals. To avoid condensation on the walls, practical experimental thermal profiles include an overheat in the vapor phase as shown in Figure 1. Unless noted, all simulations reported in this article use this thermal profile.

III. MATHEMATICAL MODEL AND NUMERICAL FORMULATION

We consider a rectangular enclosure of height H , vapor transport length L , and crystal and source material length l , where $l = L/2$ (Figure 2). The cavity's axis is inclined at an angle θ with respect to the gravitational acceleration. The solid nutrient A exists at both sides of the ampoule in equal amounts. One side is at a temperature T_S (source), the other at a temperature T_C (sink, i.e., the growing interface). With $T_S > T_C$, the compound A (mercurous chloride) sublimes from the source, is carried with a residual gas B (carbon monoxide), and condenses on the crystal interface. The source and sink interfaces are assumed to be geometrically flat. Their temperature is determined by a heat balance in the gas and the crystals. We impose the temperature profile along the upper and lower walls. The thermal conditions at the interfaces impose thermodynamically the weight fraction of component A in equilibrium with the solid through the partial pressure of the gaseous phase of compound A :

$$P_A = e^{\left[a - \frac{b}{T} \right]} \quad (1)$$

We assume complete rejection of B on both interfaces, and bounding walls are impermeable to both components. The molecular weights of the two vapor components are different, specifically one being mercurous chloride ($M_A = 472$ g/mol), the other being carbon monoxide ($M_B = 28$ g/mol). We selected carbon monoxide because it has been found experimentally to be a substantial residual vapor component⁽²⁸⁾. The viscosity and thermal conductivity are assumed to be concentration and temperature independent. The binary diffusion coefficient is taken to be pressure dependent and temperature independent.

The transport in this enclosure is governed by the system of nonlinear, coupled conservation equations for total mass (continuity), balance equation for momentum (Navier-Stokes), species mass, and energy. For a two-dimensional enclosure, and steady state conditions, the governing equations are the following:

In the vapor, ($l < x < L+l$; $0 < y < H$) ;

Continuity equation:

$$\frac{\partial(\rho u)}{\partial x} + \frac{\partial(\rho v)}{\partial y} = 0 \quad (2)$$

Momentum equations

Projection on the x axis:

$$\begin{aligned} \frac{\partial}{\partial x}(\rho uu) + \frac{\partial}{\partial y}(\rho vu) = -\frac{\partial P}{\partial x} \\ + \mu \frac{\partial}{\partial x} \left[\frac{\partial u}{\partial x} - \frac{2}{3} \left(\frac{\partial u}{\partial x} + \frac{\partial v}{\partial y} \right) \right] + \mu \frac{\partial^2 v}{\partial y \partial x} + \mu \frac{\partial^2 u}{\partial y^2} + \rho g_x \end{aligned} \quad (3)$$

Projection on the y axis:

$$\begin{aligned} \frac{\partial}{\partial x}(\rho uv) + \frac{\partial}{\partial y}(\rho vv) = -\frac{\partial P}{\partial y} \\ + \mu \frac{\partial}{\partial y} \left[\frac{\partial v}{\partial y} - \frac{2}{3} \left(\frac{\partial u}{\partial x} + \frac{\partial v}{\partial y} \right) \right] + \mu \frac{\partial^2 u}{\partial x \partial y} + \mu \frac{\partial^2 v}{\partial x^2} + \rho g_y \end{aligned} \quad (4)$$

Conservation of species equation:

$$\frac{\partial}{\partial x}(\rho u \omega_i) + \frac{\partial}{\partial y}(\rho v \omega_i) = \frac{\partial}{\partial x} \left[\rho D_{AB} \frac{\partial \omega_i}{\partial x} \right] + \frac{\partial}{\partial y} \left[\rho D_{AB} \frac{\partial \omega_i}{\partial y} \right] \quad (5)$$

Conservation of energy in the fluid phase:

$$\frac{\partial}{\partial x}(\rho u C_p T) + \frac{\partial}{\partial y}(\rho v C_p T) = \frac{\partial}{\partial x} \left[k \frac{\partial T}{\partial x} \right] + \frac{\partial}{\partial y} \left[k \frac{\partial T}{\partial y} \right] \quad (6)$$

and in the solid, ($0 < x < l$; $L+l < x < L+2l$; $0 < y < H$) :

$$\frac{\partial^2 T}{\partial x^2} + \frac{\partial^2 T}{\partial y^2} = 0 \quad (7)$$

Boundary conditions:

On the upper and lower walls, ($l < x < L+l$, $y=0$ and $y=H$), the boundary conditions of impermeability, rigidity and no-slip were used:

$$\frac{\partial \omega_i(x,0)}{\partial y} = \frac{\partial \omega_i(x,H)}{\partial y} = 0 \quad (8)$$

$$v(x,0) = v(x,H) = 0 \quad (9)$$

$$u(x,0) = u(x,H) = 0 \quad (10)$$

On the source, ($x=l$; $0 < y < H$), the diffusion of A from the source and impermeability to B were used, in addition to no-slip and an energy balance at the crystal interface:

$$u(l,y) = -\frac{D_{AB}}{1 - \omega_A(l,y)} \frac{\partial \omega_A(l,y)}{\partial x} \quad (11)$$

$$v(l,y) = 0 \quad (12)$$

$$F(l,y) - \left[k \frac{\partial T(l,y)}{\partial x} \right]_{gas} = - \left[\lambda \frac{\partial T(l,y)}{\partial x} \right]_{solid} \quad (13)$$

Analogously on the crystal, ($x = L+l$; $0 < y < H$) :

$$u(L+l,y) = - \frac{D_{AB}}{1 - \omega_A(L+l,y)} \frac{\partial \omega_A(L+l,y)}{\partial x} \quad (14)$$

$$v(L+l,y) = 0 \quad (15)$$

$$F(L+l,y) - \left[k \frac{\partial T(L+l,y)}{\partial x} \right]_{gas} = - \left[\lambda \frac{\partial T(L+l,y)}{\partial x} \right]_{solid} \quad (16)$$

The following thermal profile was used as a boundary condition along the ampoule ($y=0$, and $y=H$), (this equation is expressed in reference to an approximate fit to experimental data ⁽²⁷⁾, see Figure 1):

$$-0.10 \leq t \leq 0.22$$

$$T(t) = \begin{cases} 563.16 & -20 \leq t < -10 \text{ cm} \\ T(t) = 608. + 4.97 t - 0.70 t^2 - 5.91 \cdot 10^{-2} t^3 \\ \quad + 6.67 \cdot 10^{-3} t^4 + 2.60 \cdot 10^{-4} t^5 - 2.49 \cdot 10^{-5} t^6 & -10 \leq t \leq 12 \text{ cm} \\ 593.16 & 12 < t \leq 20 \text{ cm} \end{cases} \quad (17)$$

At the ampoule ends, the temperatures are prescribed as:

$$(x=0 ; 0 \leq y \leq H) , T=T_s ; (x=2L ; 0 \leq y \leq H) , T=T_c$$

Relative to Figure 1, during crystal growth the ampoule (Figure 2) is placed in the thermal profile. The hump region corresponds to the location of the vapor component A and B inside the ampoule. The source material lies in the region with the larger temperature near $t \geq 10 \text{ cm}$. Whereas, crystal growth occurs in the region corresponding to $t < -2 \text{ cm}$. In our numerical experiments we position the ampoule in the growth region with a temperature less than the source in order to drive the process. In addition, the length of the hump region can also be adjusted so that we have a much larger source region. With respect to Figure 2, the following transformation is used to relate the laboratory reference to the ampoule:

$$x = K_i - t$$

where K_i is the position of the source and vapor interface in the laboratory reference frame.

An energy balance at the interface between the source material and the fluid phase yields equation 13 with a source term accounting for sublimation; likewise a sink term (equation 16) also appears for the condensing interface at the crystal end. The growth rate of the interface is much smaller than the vapor velocities, typically three orders of magnitude. Thus, in comparison to the heat source term and conduction terms, the term accounting for latent heat of sublimation is negligible. This is because the product term of the growth rate and the latent heat of sublimation is negligibly

small. Also, similar to previous investigators we are considering that the interface remains flat during the growth of the crystal.

The system of coupled nonlinear partial differential equations has been solved using the SIMPLE algorithm (Semi-Implicit Method for Pressure-Linked Equations⁽³⁰⁾). The conservation equations were discretized using a hybrid scheme, which provides a second-order spatial accuracy. This two-dimensional version of the algorithm uses three staggered grids, one for the scalar variables and one for each of the velocity components. In contrast to a vorticity/stream function approach, adopting a primitive variable approach allows a straightforward formulation of the velocity boundary conditions. However, the solution of the continuity equation is no longer automatically satisfied.

For most of the simulations, a 20x60 primary grid was used. The code was run on VAX 8800 biprocessor computer, and the iterative process was stopped when a Cauchy-Schwartz type criterion was satisfied for each variable. All the results presented in this article have been obtained with a convergence criterion of 10^{-4} for each of the variables. The code was compared with a more common vorticity/stream function algorithm under the same conditions for various Grashof numbers. Results provided by the two codes differed by less than one percent⁽²⁹⁾.

IV DISCUSSION

Residual gas in PVT comes both from the process of sealing the ampoule (carbon monoxide) or later degasing of the source material. Because of the inevitable presence of this residual gas, or the introduction of a buffer gas, solutal convection can be the dominant mode of transport. The effect of the angle of tilt on solutal convection is studied. We then examine the effect of both partial pressure of carbon monoxide and mercurous chloride on the total mass flux. And conclude with a parametric study to show the levels of gravity necessary to minimize natural convection.

All simulations presented in this part are performed for an ampoule of aspect ratio of 10. The dimensionless parameters for the process under the conditions of this study are shown in table 1.

Table 1: Typical dimensionless parameters		
Thermal Grashof number	=	1050
Solutal Grashof number	=	16500
Prandtl number	=	0.7
Schmidt number	=	1
Aspect ratio	=	10
1 < Mass Peclet number < 30		

IV.1. Effect of the angle of tilt on the total mass flux in solutal convection

We now consider the effect of the angle of tilt on the total mass flux when solutal convection is dominant. We observe in Figure 3 that, for a solutal Grashof number of 1650, the maximum transport rate occurs between $30^\circ - 50^\circ$. This is in contrast to the case for thermal convection at similar Grashof numbers, considered by Markham and Rosenberger⁽¹³⁾ where the maximum occurs between $120^\circ - 135^\circ$ (depending on the aspect ratio), when the cavity is tilted toward the bottom heated configuration. There is approximately a 90° shift in maximum transport rate between thermally and

solutally dominated convection modes. This shift can be attributed to a change in transport modes between thermal and solutal convection. Note that the top heated configuration is destabilized, since we have heavy fluid over light fluid. Even though we use a steady state mathematical formulation, we are fortuitous to obtain a solution, only because we are operating below the critical Rayleigh number. For operating regions in the neighborhood of the critical Rayleigh number, a time dependent formulation and solution would be necessary.

IV.2. Effect of the partial pressure of residual gas on the total mass flux

For a given thermal boundary condition, which fixes the partial pressure of mercurous chloride at the interfaces through the vapor pressure relationship, and in the vertical configuration, we have varied the partial pressure of carbon monoxide at the evaporating interface from 0.1 Torr to 100 Torr. The evaporating interface was at a temperature of 593 ° K and the condensing interface at 563 ° K. We have taken into account the dependence of the diffusion coefficient of carbon monoxide in mercurous chloride with pressure ($D_{AB} \propto \frac{1}{P}$). The partial pressure of residual gas affects the transport rate because by increasing the partial pressure of carbon monoxide, the mass fraction of mercurous chloride at both interfaces decreases. Therefore, the mass flux is reduced. Results are shown in Figure 4. The total mass flux decreases exponentially with the partial pressure of carbon monoxide. The trend is in agreement with the experimental observations of Conder et al. ⁽¹⁸⁾ for mercurous iodide (HgI_2) and argon.

IV.3. Influence of the temperature difference on the total mass flux

The temperature difference is determined by the location of the interfaces in the thermal profile. We selected a transport length of 10 cm between the source and the crystal, and an ampoule of aspect ratio 10. A neutral position in the thermal profile for which the temperatures of the interfaces are the same can be selected. When the ampoule is positioned where the sink temperature is lower than that of the source (see Figure 1), the temperature difference drives the transport. Within the covered range the temperature difference is proportional to the distance of pulling. Figure 5 shows the interface temperature versus the distance of pulling. This figure also shows a simple relationship between the temperature difference driving transport and distance. On this basis, temperature difference and distance can be used interchangeably. The displacement of the ampoule from the neutral position is taken as the starting point for crystal growth. Thus as the crystal grows, it approaches the neutral point if the ampoule is stationary. We have computed the total mass flux versus location of the ampoule for three different partial pressures of residual gas. The results are shown in Figure 6. We notice that in all three cases the transport rate increases with temperature difference following a power law: $J_{Hg_2Cl_2} \propto \Delta T^n$ with $\frac{1}{4} \leq n \leq \frac{1}{3}$. We also observe that, as found in the previous paragraph, the total mass flux decreases with pressure of carbon monoxide, resulting in the staggering of the curves. The curves have a steep initial slope, where the exponentially increasing concentration difference drives the transfer. Then, as shown in Figure 5, as the temperature difference between source and sink approaches the neutral position, there is less driving potential for transport due to

a decrease in ΔT , thus the mass flux decreases. These results match the experimental results of Conder et al. ⁽¹⁸⁾ for a cylindrical ampoule and agree with the 1-D diffusive PVT model of Faktor and Garret ⁽²⁾.

IV.4. Effect of the temperature boundary condition

We have previously shown that when a linear axial temperature gradient is imposed on the crystal boundary ⁽²⁶⁾, a non-uniform interface temperature distribution results. This non-uniform interface temperature can induce recirculating cells in front of the interfaces. These results have been obtained for thermal convection with a linear gradient of constant sign. However, the experimental thermal profiles in our case have gradients of opposite signs at the two interfaces. The presence of the temperature peak in the middle of the ampoule destabilizes the flow in both vertical configurations for thermal convection. When considering thermal convection, density decreases with increasing temperature. Therefore, the density is smaller in the core of the ampoule than at the interfaces. As a result, both vertical configurations will be thermally unstable. Since our model problem is for steady state conditions, reliable numerical results cannot be obtained for these cases because the problem becomes unsteady.

The introduction of a temperature profile with an overheat throughout the entire vapor region does not have much effect on fluid flow pattern in tilted configurations for the case when the flow is strongly dominated by solutal convection. When solutal convection is dominant, the density gradient resulting from the mass fraction gradient stabilizes the flow in the bottom-heated configuration (Figure 7). In this case, the temperature gradient does not locally reverse the density gradient. As a result, the flow field remains stable. However, the top heated configuration remains unstable for this case. Note again that we were able to obtain a solution for this case only because we have a stabilized configuration.

IV.5. Microgravity environment

It has been shown that convection results under earthbound conditions for the horizontal configuration. Heat conduction in the crystal ⁽²⁶⁾ or internal radiative heat transfer ^(24,25) can induce convection even when the gravity vector is parallel to the longitudinal thermal gradient.

To reduce convection, one of the possible alternatives is to grow the crystal in a microgravity environment. Configurations with the g-vector perpendicular to the ampoule (i.e., horizontal configuration) have been examined for levels of gravity ranging between $10^{-6}g_0$ to $1g_0$. Figure 8 shows the variation of the total mass flux with gravity. We discern two distinct regions. Below and at $10^{-3}g_0$, the flow is diffusive. No recirculating cell is present, and the interfacial mass flux distribution is therefore planar. Above $10^{-3}g_0$, the flow switches to convective mode, and a strong recirculating cell appears, as shown in Figure 9. The corresponding streamline distribution is in Figure 10. At low gravitational acceleration, the Stefan wind drives the flow, and it is insensitive to steady levels of gravity less than $10^{-3}g_0$.

V CONCLUSIONS

Our study covers the flow field characteristics during the growth of Hg_2Cl_2 crystals in a rectangular ampoule under terrestrial and μg conditions for a nonlinear prescribed thermal gradient. Taking into account the temperature dependency of the equilibrium vapor pressure at the gas/solid interfaces reduces considerably the control we have on the process. Solutal convection is the main phenomenon governing the fluid flow inside the ampoule.

The following have been found to be evident:

1. The magnitude of convection is maximum for the top heated configuration when inclined approximately 40° .
2. The transport rate decreases exponentially with the pressure of residual gas. Pressures of carbon monoxide varying between 0.1 Torr and 100 Torr have been examined. The binary diffusion coefficient was corrected for its pressure dependency. The numerical trend is in agreement with the experimental results observed by Conder et al. ⁽¹⁸⁾.
3. The transport rate increases with the temperature difference as a power law ($J_{Hg_2Cl_2} \propto \Delta T^n$ with $\frac{1}{4} \leq n \leq \frac{1}{3}$). We have examined three different pressures of residual gas. The family of curves indicates a decrease in transport rate as residual pressure increases. Conder et al. ⁽¹⁸⁾ experimentally found the same dependency, which is also numerically predicted by the 1-D diffusive PVT model of Faktor and Garret ⁽²⁾.
4. The experimental temperature profile with an overheat in the core of the ampoule applied to avoid heterogeneous condensation of mercurous chloride on the walls, appears to destabilize the flow field when thermal convection is dominant for both vertical (0°) top-heated and (180°) bottom-heated configurations. However, when solutal convection is dominant, the density gradient resulting from the solutal concentration gradient appears to stabilize the flow in the bottom-heated configuration. The top-heated configuration becomes unstable for the case considered, solutal Grashof number in the neighborhood of 10000.
5. The microgravity environment provides a means for lowering convection. For gravity levels of $10^{-3}g_0$ or less, the Stefan wind drives the flow. No recirculating cell is predicted.

ACKNOWLEDGMENTS

This work was done while the first author held the position of Visiting Research Associate at the Universities Space Research Association. The sponsorship of both USRA and NASA Lewis Research Center are gratefully acknowledged. The authors would like to thank particularly Dr. Martin Glicksman of USRA, Dr. Mark Lee and Dr. Roger Crouch of NASA Microgravity Science and Application Division for their constant support. Mr. Thomas Glasgow, Dr. Mohammad Kassemi and Ms. Emily Nelson are thanked for their support in this work. Finally, the first author is grateful to the French Government, to the Scientific Mission in the French Embassy in Washington, to Professor Michel Gantois and to Dr. Jean-Luc Marchand for having made this stay in USA possible.

NOMENCLATURE

- a Constant term in the vapor pressure law (a=29.75)
- Ar Aspect ratio, $\left[\frac{L}{H} \right]$
- b Constant term in the vapor pressure law (b=11767.1K)
- C_p Thermal heat capacity of the gas
- D_{AB} Binary diffusion coefficient
- F(x,y) source and sink terms, $\left[= \int_0^H \rho C_p u \frac{\partial T}{\partial y} dy \right]$
- g Gravitational acceleration
- g_0 Gravitational acceleration at sea level
- Gr_t Thermal Grashof number, $\left[\frac{g \rho^2 H^3 \beta \Delta T}{\mu^2} \right]$
- Gr_s Solutal Grashof number, $\left[\frac{g \rho^2 H^3 \alpha \Delta \omega_A}{\mu^2} \right]$
- H Height of the enclosure
- J_A Mass flux of A $\left[J_A = \rho u(L+l, y) \right]$
- J_T Total mass flux of A $\left[J_T = \int_0^H \rho(L+l, y) u(L+l, y) dy \right]$
- k Thermal conductivity of the gas
- K Degree Kelvin
- L Vapor transport length
- l Length of the crystal
- M_i Molar mass of compound i
- P Pressure
- Pe Peclet number, $\left[\ln \left[\frac{P_B(L+l)}{P_B(l)} \right] \right]$
- Pr Prandtl number, $\left[C_p \frac{\mu}{k} \right]$
- R Perfect gas law constant ($R = 8.32 \text{ kgm}^2 \text{ s}^{-2} \text{ mol}^{-1} \text{ K}^{-1}$)
- Sc Schmidt number, $\left[\frac{\mu}{\rho D_{AB}} \right]$
- T Temperature
- t Coordinate attached to the laboratory reference
- u Velocity in the x-direction
- v Velocity in the y-direction

Greek symbols

α	Coefficient of solutal expansion
β	Coefficient of thermal expansion
λ	Thermal conductivity of the solid
μ	Dynamic viscosity
ω_i	Mass fraction of component i
ρ	Density of the gas
θ	Angle between the ampoule axis and the gravity vector

Subscripts

A	Compound A
B	Compound B
c	Pertains to the crystal interface
s	Pertains to the source interface
T	Total
x	Component in x direction
y	Component in y direction

Superscripts

c	Pertains to the crystal interface
s	Pertains to the source interface
*	Dimensionless

REFERENCES

1. Klosse, K.; and Ullersma, P.: Convection in a Chemical Vapor Transport Process. *J. Crystal Growth*, vol. 18, 1973, pp. 167-174.
2. Faktor, M.M.; and Garret, I.: *Growth of Crystals from the Vapour*. Chapman and Hall, London, UK, 1974.
3. Olson, J.M.; and Rosenberger, F.: Convective Instabilities in a Closed Vertical Cylinder Heated from Below. Part 1: Monocomponent Gases. *J. Fluid Mech.*, vol. 92, June 1979, pp. 609-629.
4. Olson, J.M.; and Rosenberger, F.: Convective Instabilities in a Closed Vertical Cylinder Heated from Below. Part 2: Binary Gas Mixture. *J. Fluid Mech.*, vol. 92, June 1979, pp. 631-642.
5. Rosenberger, F.: Fluid Dynamics in Crystal Growth from Vapors. *J. Phys. Chem. Hydrodynam.*, vol. 1, 1980, pp. 3-26.

6. Greenwell, D.W.; Markham, B.L.; and Rosenberger, F.: Numerical Modeling of Diffusive Physical Vapor Transport in Cylindrical Ampoules. *J. Crystal Growth*, vol. 51, 1981, pp. 413-425.
7. Markham, B.L.; Greenwell, D.W.; and Rosenberger, F.: Numerical Modeling of Diffusive-Convective Physical Vapor Transport in Cylindrical Vertical Ampoules. *J. Crystal Growth*, vol. 51, 1981, pp. 426-436.
8. Jhaveri, B.S.; Markham, B.L.; and Rosenberger, F.: On Singular Boundary Conditions in Mass Transfer Across Rectangular Enclosures. *Chem. Eng. Commun.*, vol. 13, no. 1-3, 1981, pp. 65-75.
9. Jhaveri, B.S.; and Rosenberger, F.: Expansive Convection in Vapor Transport Across Horizontal Rectangular Enclosures. *J. Crystal Growth*, vol. 57, 1982, pp. 57-64.
10. Chandra, D.; and Wiedermeier, H.: Chemical Vapor Transport and Thermal Behavior of the GeSe-Gel₄ System for Different Inclinations with Respect to the Gravity Vector; Comparison with Theoretical and Microgravity Data. *J. Crystal Growth*, vol. 57, 1982, pp. 159-176.
11. Rosenberger, F.; and Muller, G.: Interfacial Transport in Crystal Growth, a Parametric Comparison of Convective Effects. *J. Crystal Growth*, vol. 65, 1983, pp. 91-104.
12. Schiroky, G.H.; and Rosenberger, F.: Free Convection of Gases in a Horizontal Cylinder with Differentially Heated End Walls. *Int. J. Heat Mass Transfer*, vol. 27, 1984, pp. 587-598.
13. Markham, B.L.; and Rosenberger, F.: Diffusive-Convective Vapor Transport Across Horizontal and Inclined Rectangular Enclosures. *J. Crystal Growth*, vol. 67, 1984, pp. 241-254.
14. Muller, G.; Neumann, G.; and Weber, W.: Natural Convection in Vertical Bridgeman Configurations. *J. Crystal Growth*, vol. 70, 1984, pp. 78-93.
15. Schaefer, R.J.; and Coriell, S.R.: Convection-Induced Distortion of a Solid-Liquid Interface. *Metall. Trans. A.*, vol. 15A, Dec. 1984, pp. 2109-2115.
16. Huang, P.G.; Launder, B.E.; and Leschziner, M.A.: Discretization of Nonlinear Convection Processes: a Broad-Range Comparison of Four Schemes. *Comput. Methods Appl. Mech. Eng.*, vol. 48, no. 1, 1985, pp. 1-24.
17. Smutek, C., et al.: Three-Dimensional Convection in Horizontal Cylinders: Numerical Solutions and Comparison with Analytical Results. *Numer. Heat Transfer*, vol. 8, no. 5, 1985, pp. 613-631.
18. Conder, K.; Przyluski, J.; and Laskowski, J.: Vapor Transport Rate of HgI₂ in the Presence of Inert Gas. *J. Crystal Growth*, vol. 74, 1986, pp. 416-424.
19. Zappoli, B.: Interaction Between Convection and Surface Reactions in Physical Vapor Transport in Rectangular Horizontal Enclosures. *J. Crystal Growth*, vol. 76, 1986, pp. 449-461.
20. Bontoux, P., et al.: Convection in the Vertical Midplane of a Horizontal Cylinder. Comparison of Two-Dimensional Approximations with Three-Dimensional Results. *Int. J. Heat Mass Transfer*, vol. 29, Feb. 1986, pp. 227-240.

21. Henry, D.; and Roux, B.: Three-Dimensional Numerical Study of Convection in a Cylindrical Thermal Diffusion Cell: its Influence on the Separation of Constituents. *Phys. Fluids*, vol. 29, Nov. 1986, pp. 3562-3572.
22. Singh, N.B., et al.: Convection and Diffusion Effects During Physical Vapor Transport of Hg_2Cl_2 . *Materials Processing in the Reduced Gravity Environment of Space; Proceedings of the Symposium (Materials Research Society Symposia Proceedings, Vol. 87)*, R.H. Doremus and P.C. Nordine, eds., MRS, Pittsburgh, PA, 1987, pp. 71-76.
23. Extremet, G.P., et al.: Two-Dimensional Model for Thermal and Solutal Convection in a Multizone Physical Vapor Transport. *J. Crystal Growth*, vol. 82, 1987, pp. 761-775.
24. Kassemi, M.; and Duval, W.M.B.: Effect of Gas and Surface Radiation on Crystal Growth From the Vapor Phase. *J. Phys. Chem. Hydrodynam.*, vol. 11, no. 5-6, 1989, pp. 737-751.
25. Kassemi, M.; and Duval, W.M.B.: Interaction of Surface Radiation with Convection in Crystal Growth by Physical Vapor Transport. *AIAA Paper 89-0228*, 1989 (also *J. Thermophys. Heat Transfer*, vol. 4, Oct. 1989, pp. 454-461).
26. Mennetrier, C.; and Duval, W.M.B.: Thermal and Solutal Convection with Conduction Effects Inside a Rectangular Enclosure. *NASA TM-105371*, 1991.
27. Singh, N.B.; and Duval, W.M.B.: Growth Kinetics of Physical Vapor Transport Processes: Crystal Growth of the Opto-Electronic Material Mercurous Chloride. *NASA TM-103788*, 1991.
28. Singh, N.B., et al.: Purification and Characterization of Mercurous Halides. *J. Crystal Growth*, vol. 106, 1990, pp. 61-67.
29. Mennetrier, C.: Etude cinetique et modelisation du procede van Arkel. Application a la purification du hafnium. Ph.D. Dissertation, Institut National Polytechnique de Lorraine, France, 1988.
30. Patankar, S.V.: *Numerical Heat Transfer and Fluid Flow*. McGraw-Hill, New York, 1980.

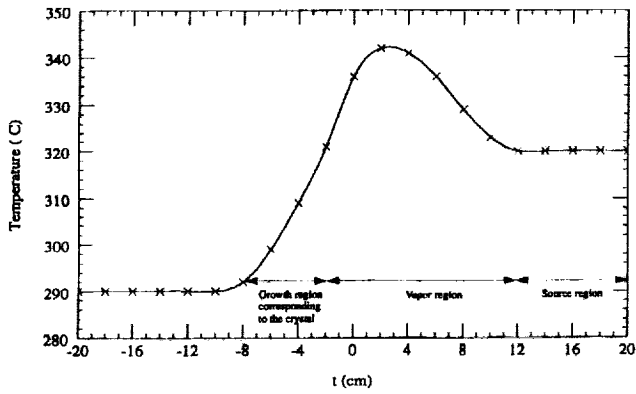


Figure 1.—Temperature profile along the ampoule.

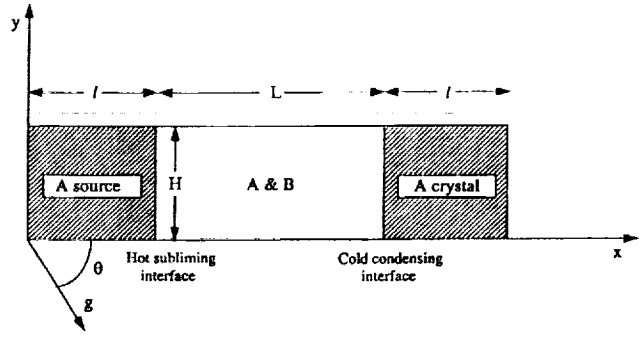


Figure 2.—Physical vapor transport enclosure.

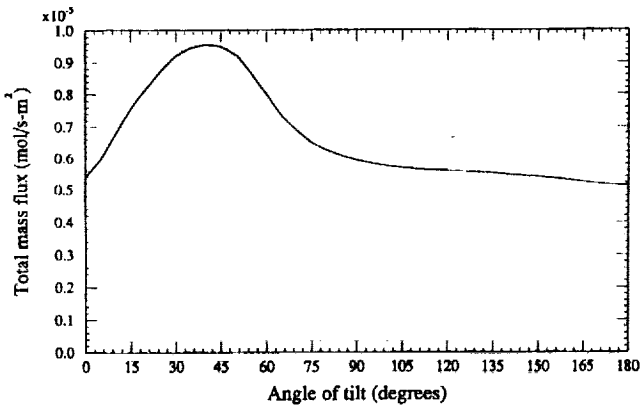


Figure 3.—Effect of angle of tilt on the total mass flux inside the enclosure ($Ar = 10$, $Gr_s = 1650$, $Gr_t = 105$, top-heated and bottom-heated configurations correspond to 0° and 180° respectively).

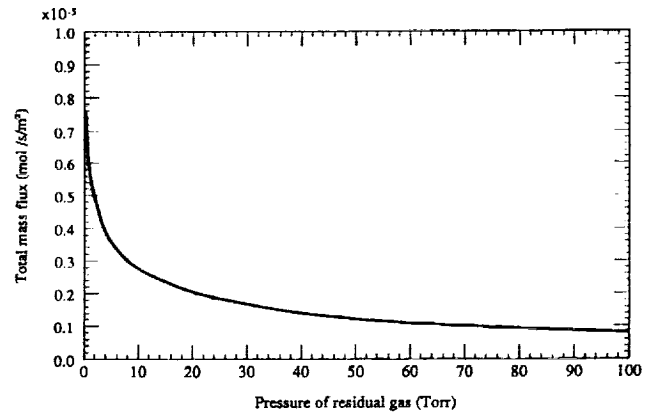


Figure 4.—Effect of the partial pressure of carbon monoxide on the total mass flux. ($Ar = 10$, vertical configuration, $Gr_s = 16500$, $Gr_t = 1050$).

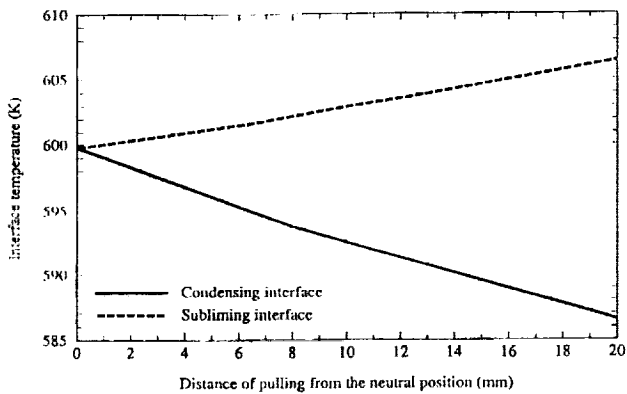


Figure 5.—Interface temperatures as a function of the distance of pulling ($L = 10$ cm, $Ar = 10$).

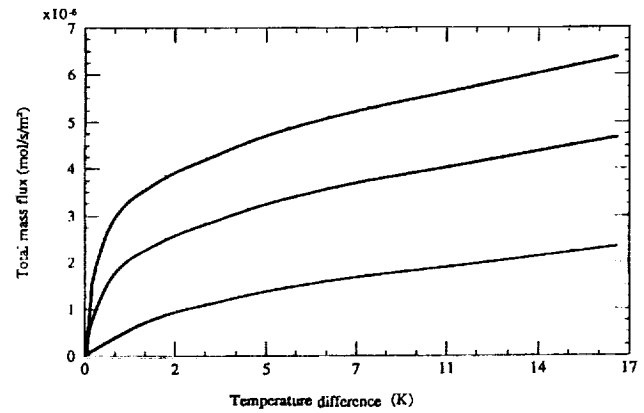


Figure 6.—Influence of the temperature difference on the total mass flux (vertical configuration, $Gr_s = 16500$, $Gr_t = 1050$, $P_{CO} = 0.2$ Torr, $P_{CO} = 1$ Torr, $P_{CO} = 10$ Torr respectively).

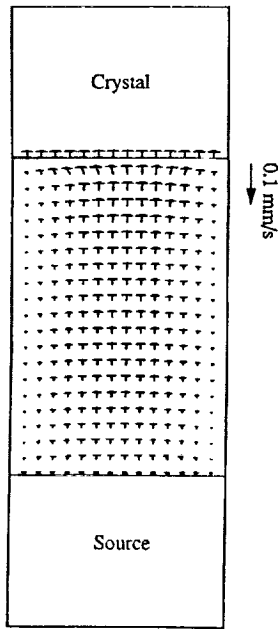


Figure 7.—Flow field in vertical configuration with experimental thermal profile ($Ar = 10$, $Gr_s = 1650$, $Gr_t = 1050$).

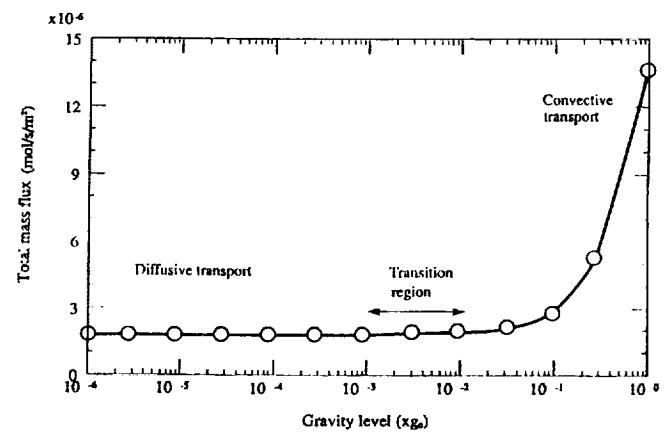


Figure 8.—Total mass flux as a function of the gravity level (horizontal configuration, $10^{-8}g_0 \leq g \leq g_0$).

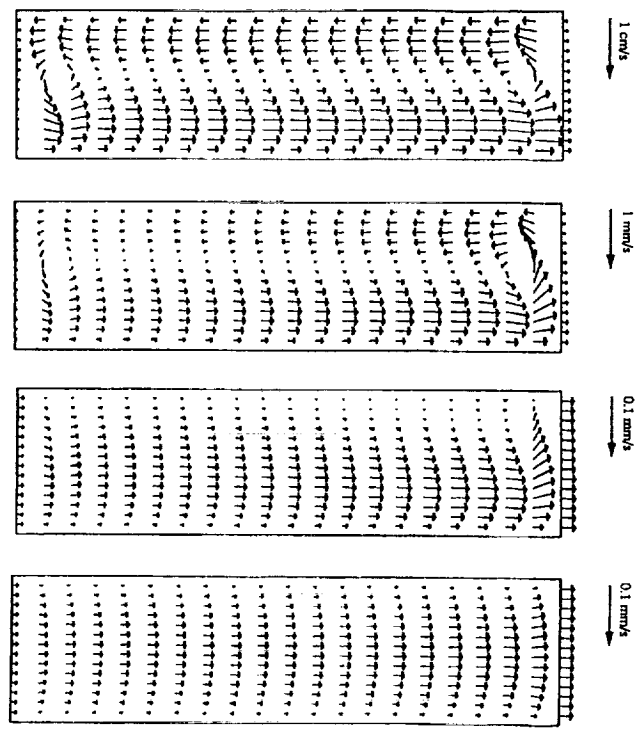


Figure 9.—Flow field for various gravitational levels (g_0 , $10^{-1}g_0$, $10^{-2}g_0$, $10^{-3}g_0$ correspond to $Gr_s = 16500$, 1650 , 165 , 16.5 respectively).

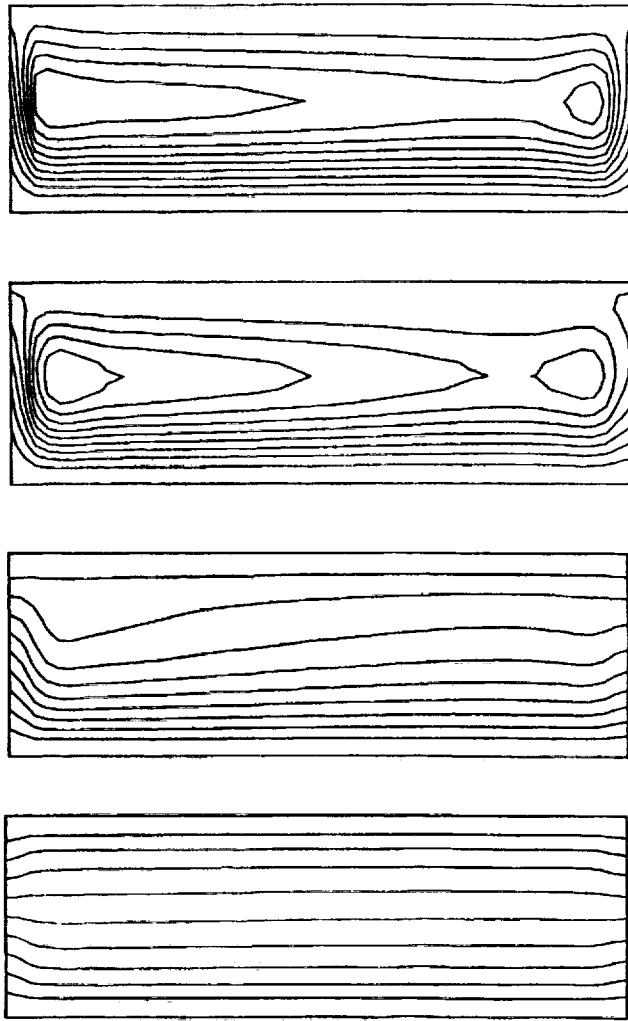


Figure 10.—Corresponding streamlines ($g_0, 10^{-1}g_0, 10^{-2}g_0, 10^{-3}g_0$ correspond to $Gr_s = 16500, 1650, 165, 16.5$ respectively).



REPORT DOCUMENTATION PAGE

Form Approved
OMB No 0704 0188

Public reporting burden for this collection of information is estimated to average 1 hour per response, including the time for reviewing instructions, searching existing data sources, gathering and maintaining the data needed, and completing and reviewing the collection of information. Send comments regarding this burden estimate or any other aspect of this collection of information, including suggestions for reducing this burden, to Washington Headquarters Services, Directorate for Information Operations and Reports, 1215 Jefferson Davis Highway, Suite 1204, Arlington, VA 22202 4302, and to the Office of Management and Budget, Paperwork Reduction Project (0704 0188), Washington, DC 20503

1. AGENCY USE ONLY (Leave blank)		2. REPORT DATE November, 1992	3. REPORT TYPE AND DATES COVERED Technical Memorandum	
4. TITLE AND SUBTITLE Physical Vapor Transport of Mercurous Chloride Under a Nonlinear Thermal Profile			5. FUNDING NUMBERS WU-674-21-05	
6. AUTHOR(S) Christophe Mennetrier, Walter M.B. Duval, and Narsingh B. Singh				
7. PERFORMING ORGANIZATION NAME(S) AND ADDRESS(ES) National Aeronautics and Space Administration Lewis Research Center Cleveland, Ohio 44135-3191			8. PERFORMING ORGANIZATION REPORT NUMBER E-7413	
9. SPONSORING/MONITORING AGENCY NAMES(S) AND ADDRESS(ES) National Aeronautics and Space Administration Washington, D.C. 20546-0001			10. SPONSORING/MONITORING AGENCY REPORT NUMBER NASA TM-105920	
11. SUPPLEMENTARY NOTES Christophe Mennetrier, Walter M.B. Duval, NASA Lewis Research Center, Cleveland, Ohio and Narsingh B. Singh, Westinghouse Science and Technology Center, Pittsburgh, Pennsylvania. Responsible person, Walter M.B. Duval, (216) 433-5023.				
12a. DISTRIBUTION/AVAILABILITY STATEMENT Unclassified - Unlimited Subject Category 34 and 64			12b. DISTRIBUTION CODE	
13. ABSTRACT (Maximum 200 words) Our study investigates numerically the flow field characteristics during the growth of mercurous chloride (Hg_2Cl_2) crystals in a rectangular ampoule under terrestrial and μg conditions for a nonlinear thermal gradient. With a residual gas lighter than the nutrient, the solutal Grashof number is dominant. We observe that in tilted configurations, when solutal convection is dominant, the maximum transport rate occurs at approximately 40° . For the vertical configurations, we were able to obtain solutions only for the cases either below the critical Rayleigh numbers or the stabilized configurations. The total mass flux decreases exponentially with an increase of pressure of residual gas, but it increases following a power law with the temperature difference driving the transport. The nonlinear thermal gradient appears to destabilize the flow field when thermal convection is dominant for both vertical top-heated and bottom-heated configurations. However, when the solutal Grashof number is dominant, the density gradient resulting from the solutal gradient appears to stabilize the flow for the bottom-heated configuration. The flow field for the top-heated configuration is destabilized for high Grashof numbers. The microgravity environment provides a means for lowering convection. For gravity levels of $10^{-3} g_0$ or less, the Stefan wind drives the flow, and no recirculating cell is predicted.				
14. SUBJECT TERMS Physical vapor transport; Mercurous chloride; Crystal growth			15. NUMBER OF PAGES 18	
			16. PRICE CODE A03	
17. SECURITY CLASSIFICATION OF REPORT Unclassified	18. SECURITY CLASSIFICATION OF THIS PAGE Unclassified	19. SECURITY CLASSIFICATION OF ABSTRACT Unclassified	20. LIMITATION OF ABSTRACT	